Fish and Shellfish Immunology 120 (2022) 547–559

Contents lists available at ScienceDirect

Fish and Shellfish Immunology

journal homepage: www.elsevier.com/locate/fsi

Blood cell characterization and transcriptome analysis reveal distinct immune response and host resistance of different ploidy cyprinid fish following *Aeromonas hydrophila* infection

Ning-Xia Xiong [a], Jie Ou [a], Lan-Fen Fan [b], Xu-Ying Kuang [a], Zi-Xuan Fang [a], Sheng-Wei Luo [a,*], Zhuang-Wen Mao [c], Shao-Jun Liu [a,**], Shi Wang [a], Ming Wen [a], Kai-Kun Luo [a], Fang-Zhou Hu [a], Chang Wu [a], Qing-Feng Liu [a]

[a] State Key Laboratory of Developmental Biology of Freshwater Fish, College of Life Science, Hunan Normal University, Changsha, 410081, PR China
[b] College of Marine Sciences, South China Agricultural University, Guangzhou, 510642, PR China
[c] Hunan Provincial Key Laboratory of Nutrition and Quality Control of Aquatic Animals, Department of Biological and Environmental Engineering, Changsha University, Changsha, 410022, PR China

ARTICLE INFO

Keywords:
Hybrid fish
Transcriptome
Gene expression
Aeromonas hydrophila

ABSTRACT

Aeromonas hydrophila can pose a great threat to survival of freshwater fish. In this study, *A. hydrophila* infection could decrease blood cell numbers, promote blood cell damage as well as alter the levels of alkaline phosphatase (ALP), lysozyme (LZM), aspartate aminotransferase (AST), total antioxidant capacity (T-AOC), total superoxide dismutase (SOD), catalase (CAT) and malondialdehyde (MDA) in immune-related tissues of red crucian carp (RCC, 2 N = 100) and triploid cyprinid fish (3 N fish, 3 N = 150). In addition, the significant alternation of antioxidant status was observed in PBMCs isolated from RCC and 3 N following LPS stimulation. The core differential expression genes (DEGs) involved in apoptosis, immunity, inflammation and cellular signals were co-expressed differentially in RCC and 3 N following *A. hydrophila* challenge. NOD-like receptor (NLR) signals appeared to play a critical role in *A. hydrophila*-infected fish. DEGs of NLR signals in RCCah vs RCCctl were enriched in caspase-1-dependent Interleukin-1β (IL-1β) secretion, interferon (IFN) signals as well as cytokine activation, while DEGs of NLR signals in 3Nah vs 3Nctl were enriched in caspase-1-dependent IL-1β secretion and antibacterial autophagy. These results highlighted the differential signal regulation of different ploidy cyprinid fish to cope with bacterial infection.

1. Introduction

Triploidization is generally considered to be the practical and effective strategy for large-scale generation of sterile fish, which presents a great economic importance to fish farming [1]. However, artificial induction of triploidy fish by pressure or temperature shock may lower the disease resistance, decrease weight gains and enhance rates of vertebral compression [2]. Hybridization may refer to the crossbreeding of different species or higher ranking taxa, which can lead to production of novel genotypes and phenotypes in hybrid offsprings [3] and give rise to species with novel capabilities [4]. Chimeric genes and non-synonymous mutation in hybrid offsprings may generate structural changes at transcriptional level that can alter gene expressions, enzymatic activities and cellular signals upon stimulation [5]. Recent reports suggest that hybrid fish can elicit a low susceptibility to pathogenic infection by comparing with those of their parental species [6].

Crucian carp (*Carassius auratus*) is one of the most important economic freshwater fish and abundant in lakes, rivers and reservoirs in China, which is popular with fish farmers [7]. The bisexual fertile tetraploid cyprinid fish (4 N = 200) were generated by intergeneric hybridization of red crucian carp (RCC, *Carassius auratus* red var, 2 N = 100, ♀) and common carp (CC, *Cyprinus carpio* L, 2 N = 100, ♂) [8,9]. Then, sterile triploid fish (3 N = 150) were obtained by crossing of RCC (2 N = 100, ♀) and allotetroploid fish (4 N = 200, ♂) [10]. Triploid fish (3 N fish) contained two sets of RCC chromosome groups and one set of CC chromosomes, which may provide an animal model for studying

* Corresponding author. College of Life Science, Hunan Normal University, Changsha, 410081, PR China.
** Corresponding author. College of Life Science, Hunan Normal University, Changsha, 410081, PR China.
E-mail addresses: swluo@hunnu.edu.cn (S.-W. Luo), lsj@hunnu.edu.cn (S.-J. Liu).

https://doi.org/10.1016/j.fsi.2021.12.024
Received 5 October 2021; Received in revised form 14 December 2021; Accepted 15 December 2021
Available online 17 December 2021

sterility, growth, and disease resistance mechanism.

Innate immunity of fish serves as the first line of defense against pathogenic infection, possessing developed complement systems, immune-related pathways as well as various forms of pathogen-recognizing properties [11,12]. Increasing studies demonstrate that environmental pollution can exhibit an immunosuppressive effect in fish [13]. In general, invading pathogens successfully breach mucosal and epithelial barriers that can cause inflammatory events, whilst a large range of cell types and signal mediators are involved in pathogen-induced inflammatory response [14]. *Aeromonas hydrophila*, a gram-negative pathogen, is a widespread representative of *Aeromonadaceae* found in water, river sediment, fish and shellfish, which can generate various virulence factors [15]. *Aeromonas* spp. contains heat-labile cytotonic and heat-stable cytotonic enterotoxin, which is highly associated with the occurrences of watery diarrhoea [16]. Apart from documented problems, crucian carp is ravaged by water-borne pathogenic diseases, posing a great threat to the survival of aquatic animals [17,18]. *A. hydrophila* infection (1×10^8 CFU ml^{-1}) can sharply increase accumulative mortality of allogynogenetic crucian carp [19]. In our previous studies, we found that erythrocytes of 3 N exhibited a stronger resistance against *A. hydrophila*-induced hemolysis by comparing with those of RCC [20]. However, the differential regulation in immune signals of different ploidy cyprinid fish following *A. hydrophila* challenge were unclear.

In this study, the aims were to study cell morphology and transcriptome analysis in peripheral whole blood from RCC and 3 N. To further characterize their functions, peripheral blood mononuclear cells (PBMCs) were isolated for assessment of immune-related properties upon stimulation, which may provide a new insight into immune regulation in peripheral blood of different ploidy cyprinid fish.

2. Materials and methods

2.1. Animals

RCC and 3 N (average length 16.8 ± 0.92 cm) were obtained from an aquaculture base in Wang Cheng district (Changsha, China) and acclimatized in 70 × 65 × 65 cm plastic aquarium (25 fishes/aquarium) with the diluted freshwater (pH 8.0, 23 ± 1 °C) for two weeks and fed with commercial diet twice daily till 24 h before challenge experiment, respectively. In addition, water quality was properly controlled to avoid pathogenic contamination during fish acclimation or immune challenge.

2.2. Immune challenge with A. hydrophila

A. hydrophila was cultured for 24 h at 28 °C, centrifuged at 10000×*g* for 15 min at 4 °C, and resuspended in 1 × PBS (pH 7.3). 100 μl suspension of 1×10^8 CFU ml^{-1} *A. hydrophila* in phosphate buffered saline (PBS) was injected intraperitoneally, which was served as infection group (RCCah and 3Nah). In contrast, injection of 100 μl sterile PBS was used as the control group (RCCctl and 3Nctl). Peripheral blood samples were withdrawn from caudal veins of RCC and 3 N fish at 8 h post-infection. The isolated peripheral blood, head kidney and spleen were immediately frozen in liquid nitrogen and preserved in −80 °C. Three sets of peripheral blood RNA for each group for biological replication and each set of RNA was pooled RNA extracted from peripheral blood of three individuals for RNA-seq library construction. Meanwhile, pooled RNA isolated from several immune-related tissues from 3 N was used for PacBio SMRT sequencing.

2.3. Blood cell counts

A drop of diluted blood samples from each group was placed on the hemocytometer and counted by using a light microscope. The experiment was performed in triplicate.

2.4. Blood smear assay

The above diluted blood samples were smeared uniformly across a cover glass by using another cover glass. After 10 min air-drying at room temperature, blood samples were stained with Giemsa staining kit. Following rinsing with deionized water, cover glasses were observed using a light microscope. Then, the percentage of undamaged cells were calculated. The experiment was performed in triplicate.

2.5. PacBio iso-seq, data processing, functional annotation and structure analysis

Total RNA was isolated from 3 N by TRIzol® Reagent (Invitrogen, USA) and used for PacBio library construction. After purification and adapter ligation, sequencing reactions were performed by PacBio Sequel sequencer. Sequencing raw data were processed by using SMRTlink 8.0 pipeline. Circular consensus sequence (CCS) was produced from subread BAM files. Then, the classification of full length (FL) reads and non-full length (NFL) reads were performed by identifying 5′ adapters, 3' adapters and poly (A) tail. The accuracy of consensus isoforms was subjected to isoform-level clustering (ICE) and final polishing by arrow algorithm. Transcriptome completeness was benchmarked by using Benchmarking Universal Single-Copy Orthologs (BUSCO). The obtained genes or transcripts were blasted against seven nucleotide and protein databases, including NCBI non-redundant proteins (NR), nucleotide database (NT), non-redundant protein database (Swiss-prot), conserved protein families or domains (Pfam), clusters of orthologues groups of proteins (KOG/COG), kyoto encyclopedia of genes and genomes (KEGG) and gene ontology (GO). Corrected P-value < 0.05 were thought to be significantly enriched.

Alternative splicing (AS) and alternative polyadenylation (APA) were predicted by using TAPIS pipeline. Simple sequence repeat (SSR) was analyzed by using MicroSAtellite identification tool. Transcription factor (TF) identification and transcripts assignment were analyzed by algorithm Hmmscan software compared with AnimalTFDB 2.0 database. For long non-coding RNA (lncRNA) analysis, Pfam, coding-non-coding-index (CNCI), coding potential calculator (CPC), and coding potential assessment tool (CPAT) were used for coding prediction of transcripts.

2.6. RNA sequencing, DEGs identification and gene co-expression network analysis

Total RNA was extracted from RCC and 3 N, respectively. After quality check, total RNA was enriched from each sample for cDNA construction. Following adapter ligation, purified cDNA was selected for PCR amplification by using Illumina HiSeq 2500 platform. Clean reads were obtained after the removal of raw reads containing adapter contaminants, reads with more than 10% N (unknown nucleotides) and low-quality reads. The remaining high-quality clean reads of 3 N were mapped to PacBio reference sequence, while RCC clean reads were mapped to the reference genome of *Carassius auratus* red var using HISAT software with default parameters [21].

Expression levels of DEGs were quantified according to fragments per kilobase of transcript per million mapped reads (FPKM) values by using HTSeq software, which was subjected to principal component analysis (PCA). Statistical analysis of DEGs was performed among groups by using DESeq2 assay and screened with the threshold values of false discovery rate <0.05. Clustering analysis was performed by using Pheatmap package in R based on FPKM of DEGs. DEGs were analyzed by GO and KEGG. Then, annotated DEGs were selected to construct gene co-expression network via parmigene package in R.

2.7. Quantitative real-time PCR (qRT-PCR) validation

Interleukin-8 (IL-8), C-X-C motif chemokine receptor 1 (CXCR1), toll-like receptor 5 (TLR5), C-type lectin domain containing 9A

(CLEC9A), Interleukin-1β (IL-1β), Cluster of differentiation 81 (CD81), Natural killer lysin (NK-lysin) and Ferritin M (FerM) were selected for RNA-seq results by using qRT-PCR assay. In brief, cDNA synthesis was performed by using Revert AidTM M-MuLV Reverse Transcriptase Kit (MBI Fermentas, USA). 18S rRNA was used as internal control. Primers used in this study were shown in Table 1. Primer specificity was confirmed and each sample was analyzed in triplicate. At the end of qRT-PCR assay, melting curve analysis was implemented to confirm credibility of each qRT-PCR analysis. Results were measured by using Applied Biosystems QuantStudio 5 Real-Time PCR System with $2^{-\triangle\triangle Ct}$ methods.

2.8. Enzymes and lipid peroxidation assay

2.8.1. Detection of alkaline phosphatase (ALP) activity

The isolated liver, head kidney, trunk kidney and spleen of RCC and 3 N were homogenized on ice-cold 1 × PBS buffer. Following centrifugation at 10000×*g* for 10 min at 4 °C, the supernatants were obtained and quantified by using bicinchoninic acid (BCA) method. According to protocol of alkaline phosphatase (ALP) activity kit (Nanjing Jiancheng Bioengineering institute, China), ALP activities in the supernatants of tissue homogenates were measured. The reaction compounds could be detected by the absorbance at 520 nm. Then, results were expressed as mU ALP activity per milligram of protein. The experiment was performed in triplicate.

2.8.2. Detection of aspartate aminotransferase (AST) activity

According to protocols, AST activities in above supernatants of tissue homogenates were measured by using aspartate aminotransferase (AST) activity kit (Nanjing Jiancheng Bioengineering institute, China). The reaction compounds could be detected by the absorbance at 510 nm. Then, results were expressed as mU AST per milligram of protein. The experiment was performed in triplicate.

2.8.3. Detection of lysozyme (LZM) activity

According to previous studies, LZM activities in above supernatants of tissue homogenates were measured [22]. In brief, 0.02% (w/v) suspension of *Micrococcus lysodeikticus* (Sigma-Aldrich, Inc, USA) in 0.05 M phosphate buffer (pH 6.2) was used as substrate, while lyophilized hen egg white lysozyme was used as a standard. The supernatants of tissue homogenates were added to the substrate at 25 °C. The results of enzymatic activity were expressed as U LZM activity per milligram of protein. The experiment was performed in triplicate.

2.8.4. Detection of total superoxide dismutase (SOD) activity

Based on the protocol of total SOD activity kit (Beyotime Biotechnology, Shanghai, China), the enzymatic activities in above supernatants of tissue homogenates were measured as the changes in absorbance at 560 nm by using a microplate reader. The results were given in units of SOD activity per milligram of protein, where 1 U of SOD is defined as the amount of enzyme producing 50% inhibition of SOD. The experiment was repeated in triplicate.

Table 1
The primer sequences used in this study.

Primer names	Sequence direction (5′ → 3′)	Use
RT-18S–F	CCGACCCTCCCTCACG	qPCR
RT-18S-R	GCCTGCTGCCTTCCTTG	qPCR
RT -CD81-F	GAAGGGAATCAGGCACCAG	qPCR
RT -CD81-R	CCACCTCACAGGCGAAGA	qPCR
RT -CXCR1-F	AGACGATGCTTTGCTCCC	qPCR
RT -CXCR1-R	GCCTACGATCAGATTCCCAG	qPCR
RT -CLEC9A-F	CGAGGAGTCTGTTTATGCGG	qPCR
RT -CLEC9A-R	AAAGCGGCTCTTCTTCAGTATG	qPCR
RT -TLR5-F	GAAACCTTCAACCTGGCTCA	qPCR
RT -TLR5-R	ATCCTGGCTGTCGTCGG	qPCR
RT -IL8-F	CTTCCCTCCAAGCCCACA	qPCR
RT -IL8-R	TCTCAATGACCTTCTTTACCCA	qPCR
RT-FerM-F	TCAGGTTCGCCAAAACTACG	qPCR
RT-FerM-R	CCATTGTCCCACTCATCGC	qPCR
RT-NK-lysin-F	TGCGGAGAATCGTCGTG	qPCR
RT-NK-lysin-R	GGTTTTGGCGTCATCAGTAG	qPCR
RT-IL-1β-F	CCTGACAGTGCTGGCTTTG	qPCR
RT-IL-1β-R	AATGATGATGTTCACCACCTTC	qPCR

2.8.5. Detection of catalase (CAT) activity

Measurement of CAT activity was performed according to ammonium molybdate spectrophotometric method. Based on protocol of CAT activity kit (Nanjing Jiancheng Bioengineering Institute, Nanjing, China), the reaction compounds could be monitored by the absorbance at 405 nm. The results of enzymatic assays were given in units of CAT activity per milligram of protein, where 1 U of CAT is defined as the amount of enzyme decomposing 1 μmol H_2O_2 per second. The experiment was repeated in triplicate.

2.8.6. Detection of total antioxidant capacity (T-AOC)

Total antioxidant capacity (T-AOC) can be expressed in term of the contribution to antioxidant compounds when taking into account varied rates of antioxidant reaction with 2,2′-azinobis-(3-ethylbenzthiazoline-6-sulphonate) (ABTS). According to protocol of T-AOC assay kit with ABTS method (Beyotime Biotechnology, Shanghai, China), T-AOC levels were measured. Trolox solution was used as a reference standard. Quenching of the cation can be measured at 734 nm by using a Synergy 2 multi-detection microplate reader (Bio-Tek, USA). Results were expressed as micromole T-AOC per milligram of protein. The experiment was repeated in triplicate.

2.8.7. Detection of malondialdehyde (MDA) amount

Free MDA and lipid hydroperoxides can be selected determined by thiobarbituric acid (TBA) method. According to protocol of lipid peroxidation MDA assay kit (Beyotime Biotechnology, Shanghai, China), MDA amounts in the supernatants of tissue homogenates were measured. Results were expressed as nanomole MDA per milligram of protein. The experiment was repeated in triplicate.

2.9. Biochemistry analysis of peripheral blood mononuclear cells (PBMCs)

2.9.1. PBMCs isolation in vitro

According to previous studies, PBMCs isolation was performed [23]. In brief, peripheral blood was collected from caudal vessels from RCC and 3 N, diluted in PBS and then gently loaded onto a discontinuous gradient consisting of 10 ml 54% percoll (Sigma, USA) and overlaid with 10 ml of 31% percoll. After centrifugation at 600×*g* for 40 min, PBMCs were collected from 31 to 54% interface, washed with Dulbecco's modified eagle medium (DMEM) and resuspended in DMEM containing 10% fetal bovine serum (FBS). Cell viability was determined by trypan blue staining and cell number was adjusted for following analyses.

2.9.2. Cell viability of PBMCs following lipopolysaccharide (LPS) stimulation

To detect the potential effect of LPS stimulation on the cell viability, cell counting kit-8 (CCK-8, Beyotime Biotechnology, Shanghai, China) assay was performed. In brief, above isolated PBMCs were seeded in 96-well plate and treated with 1000 ng/ml of LPS. Then, 10 μl of CCK-8 solution was added to each well and the optical density was measured at 450 nm. The experiment was performed in triplicate.

2.9.3. Measurement of reactive oxygen species (ROS) in PBMCs following LPS stimulation

To investigate the intracellular ROS content generated by LPS stimulation, DCFH-DA probe (Beyotime Biotechnology, Shanghai, China) was used. In brief, above isolated PBMCs were pretreated with N-Acetyl-L-cysteine (NAC, 4 mM) for 30 min and incubated with 1000 ng/ml of

LPS for 24 h and 48 h. Following incubation with DCFH-DA probe, cells were washed twice with PBS. Fluorescence values were detected by using a Synergy 2 multifunctional microplate reader (Bio-Tek, USA). The experiment was performed in triplicate.

2.9.4. Measurement of antioxidant status in PBMCs following LPS stimulation

Total SOD activities, NADPH/$NADP^+$ contents and malondialdehyde (MDA) productions were measured based on previous studies [24]. Briefly, above isolated PBMCs were treated with 1000 ng/ml LPS and sampled at 0, 6, 12, 24 and 48 h. After that, cells were harvested, homogenized with ice-cold PBS and centrifuged at 12,000×*g* for 10 min at 4 °C. Protein concentrations in supernatants of cell lysate samples were determined by using BCA method. Total SOD activities in PBMCs were measured by using total superoxide dismutase (SOD) activity kit (Beyotime Biotechnology, Shanghai, China). Results were given in units of SOD activity per milligram of protein, where 1 U of SOD is defined as the amount of enzyme producing 50% inhibition of SOD. NADPH/$NADP^+$ contents in PBMCs were determined by using NADPH/$NADP^+$ assay kit (Beyotime Biotechnology, Shanghai, China). Results were expressed as micromole NADPH/$NADP^+$ per milligram of protein. MDA amounts in PBMCs were detected by using lipid peroxidation MDA assay kit (Beyotime Biotechnology, Shanghai, China). Results were expressed as nanomole MDA per milligram of protein. The experiment was repeated in triplicate.

2.10. Statistical analyses

The data analysis was measured by using SPSS 18 analysis program and represented as means ± standard deviation. All of the experimental data analyses were subjected to Student's *t*-test or one-way ANOVA (one-way analysis of variance). Further analysis of Duncan's multiple range test, only if the level of P-value < 0.05, the differences were considered statistically significant.

3. Results

3.1. PacBio Iso-seq and bioinformatic analysis

Raw reads generated by PacBio Iso-seq were filtered for a clean data, resulting in a total of 41.39 GB subreads with a mean CCS read length of 2421 bp. A total of 551223 CCS reads were obtained for classification of FL and NFL iso-forms, showing that 443746 (80.50%) CCS reads were classified as full-length non-chimeric reads (FLNCs). FLNCs clustering analysis revealed that the obtained FLNCs harbored 180795 consensus sequences with the average length of 2730 bp, which contained 170002 polished high-quality isoforms (Supplementary Figs. 1A–B). In Supplementary Fig. 1C, BUSCO analysis revealed that 71.8% of BUSCO genes of 3 N were detected in our transcriptome.

AS and APA can promote transcript diversity, gene complexity and metabolic flow in organisms. In Fig. 1A-B, a total of 29142 AS events were identified in full-length transcripts of 3 N, consisting of alternative 3′ splice site (13.71%), alternative 5' splice site (9.43%), exon skipping (16.55%), intron retention (58.60%) and mutually exclusive exon (1.71%). In Fig. 1C, the results showed that 7897, 2456, 926, 376 and 157 transcripts contained at least one, two, three, four and five poly (A) sites, respectively, which resulted in a total of 11974 APA events. SSR can modify gene regulation, transcription and protein function, playing an important role in generation of genetic variation. The varied types of SSR density distribution were shown in Fig. 1D. A total of 121141 SSRs were identified from 85061 examined sequences with the highest SSR density of mononucleotides, containing 64032 mononucleotides, 43404 dinucleotide, 11659 trinucleotide, 1704 tetranucleotide, 277 pentanucleotide and 65 hexanucleotide. In Fig. 1E, a total of 11737 TFs were identified in full-length transcripts of 3 N with the highest abundance of zf-C2H2. In Fig. 1F-G, a total of 9821 lncRNA sequences were identified by using CNCI, CPC, Pfam and CPAT, including 2254 large intergenic non-coding RNA (lincRNA) sequences, 456 antisense-lncRNA sequences, 3162 intronic-lncRNA sequences and 3751 sense-lncRNA sequences.

In this study, a total of 86548 transcripts were obtained by removing redundancy of high quality consensus sequences. In addition, a total of 45805 full-length open reading frame (ORF) sequences were identified from assembled transcript data and functional annotation of 52829 new transcripts were completed (Supplementary Fig. 2A). To obtain comprehensive analysis of gene function in 3 N, a total of 52829 new isoforms were aligned to seven different nucleotide and protein databases (Supplementary Fig. 2B). In Fig. 2A, a total of 41220 new isoforms were annotated by GO. In cellular component category, the predominant portion of transcripts represented "cell" (20844), followed by "cell parts" (20797) and "organelle" (12913). In molecular function category, "binding" (19743) and "catalytic activity" (11871) were the most abundant sub-categories. In biological process category, the sub-categories of "cellular process" (21183), "single-organism process" (18775) and "biological regulation" (15559) were the major portions of transcripts. In Fig. 2B, KOG analysis revealed that the largest cluster was "General function prediction only" (8189), followed by "Signal transduction mechanism" (7889).

3.2. Comparative analysis of blood cell number and morphology in different ploidy cyprinid fish following A. hydrophila challenge

The ploidy of RCC and 3 N was determined prior to functional analysis as previously described [20]. In Fig. 3A, blood cell numbers decreased significantly in RCC and 3 N subjected to *A. hydrophila* challenge. In Fig. 3B, *A. hydrophila* challenge could promote nuclear enlargement, generate cytoplasmic vacuoles and cause abnormal nucleocytoplasmic ratios in blood cells of RCC and 3 N following *A. hydrophila* challenge by comparing with their respective controls. In Fig. 3C, percentages of undamaged blood cells were approximately 37.01% and 65.47% in RCC and 3 N following *A. hydrophila* challenge, respectively.

3.3. Enzymatic activity and antioxidant status following A. hydrophila challenge

Enzymatic activities of ALP, AST, LZM in RCC and 3 N were investigated following *A. hydrophila* challenge. As shown in Fig. 4A, ALP activities increased dramatically in liver, head kidney, trunk kidney and spleen of 3 N following *A. hydrophila* challenge. In contrast, elevated levels of ALP activities were observed in liver, head kidney and spleen of RCC following *A. hydrophila* challenge, while it decreased sharply in trunk kidney. In Fig. 4B, splenic AST activity increased sharply in RCC subjected to *A. hydrophila* infection, while AST activities decreased significantly in liver and trunk kidney. In contrast, up-regulated levels of AST activities were observed in head kidney and spleen of 3 N following *A. hydrophila* challenge, while it decreased significantly in trunk kidney. In Fig. 4C, *A. hydrophila* challenge could sharply decrease LZM activities in liver, trunk kidney and spleen of RCC and 3 N, while LZM activity in head kidney of RCC and 3 N increased significantly.

Antioxidant parameters in RCC and 3 N following *A. hydrophila* challenge were shown in Fig. 4D–G. In Fig. 4D, total SOD activity increased sharply in spleen of RCC following *A. hydrophila* challenge, while decreased levels of total SOD activities were observed in liver, head kidney and trunk kidney. In contrast, total SOD activities increased significantly in head kidney and spleen of 3 N following *A. hydrophila* challenge, while it decreased dramatically in liver and trunk kidney. In Fig. 4E, RCC receiving *A. hydrophila* exhibited a sharp decrease of CAT activities in liver, head kidney, trunk kidney and spleen. In contrast, CAT activities increased dramatically in head kidney and trunk kidney of 3 N following *A. hydrophila* challenge, whereas it decreased significantly in liver and spleen. In Fig. 4F, down-regulation of T-AOC levels was detected in liver, trunk kidney and spleen of RCC after *A. hydrophila*

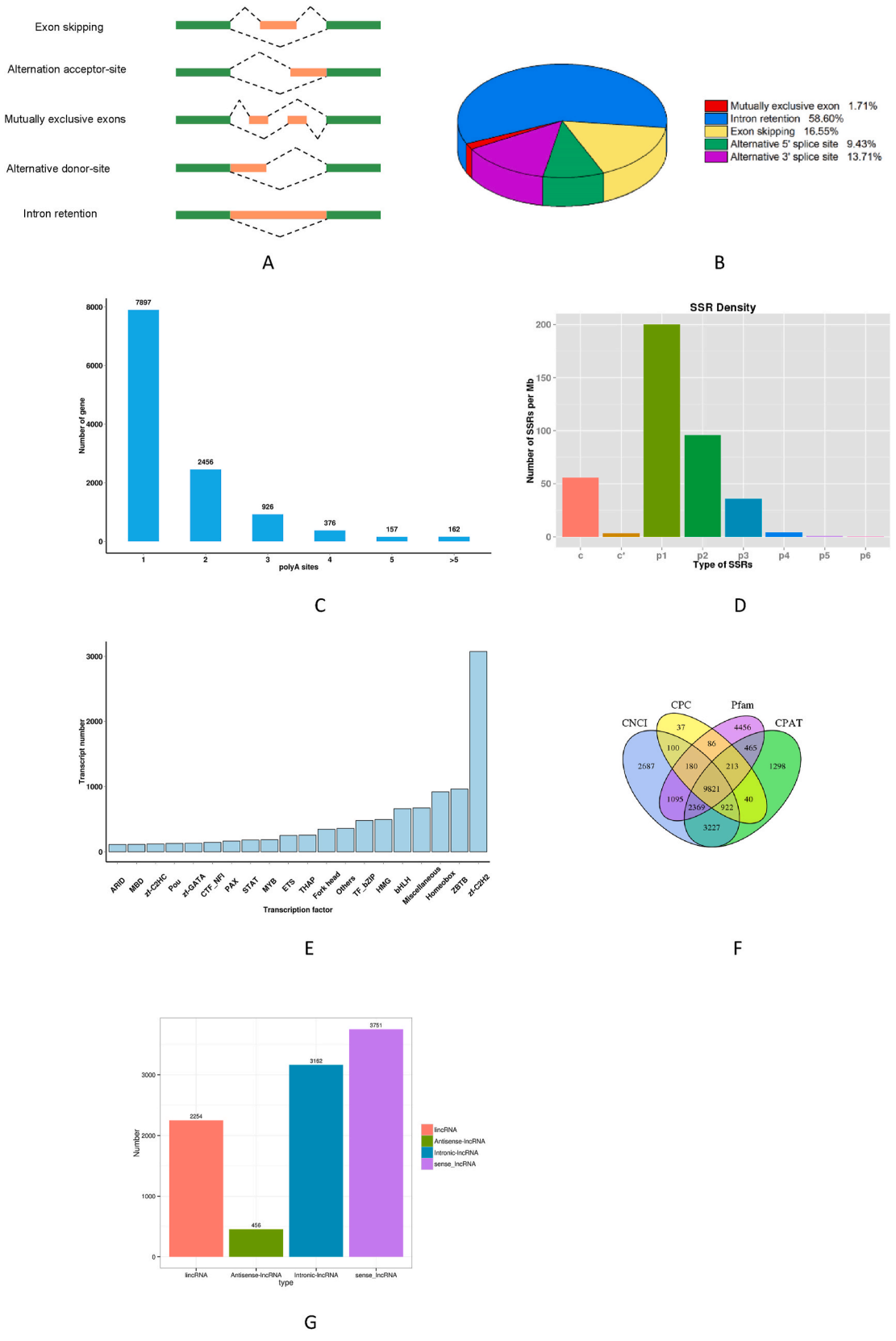

Fig. 1. Functional annotation and structure analysis in 3 N full-length transcriptome. (A) Different kinds of AS events. (B) Statistic results of AS events. (C) Numbers of APA events. (D) Numbers of SSRs. (E) Numbers of TFs. (F) Venn diagram of lncRNA prediction results. (G) Statistical graph of lncRNA classification results.

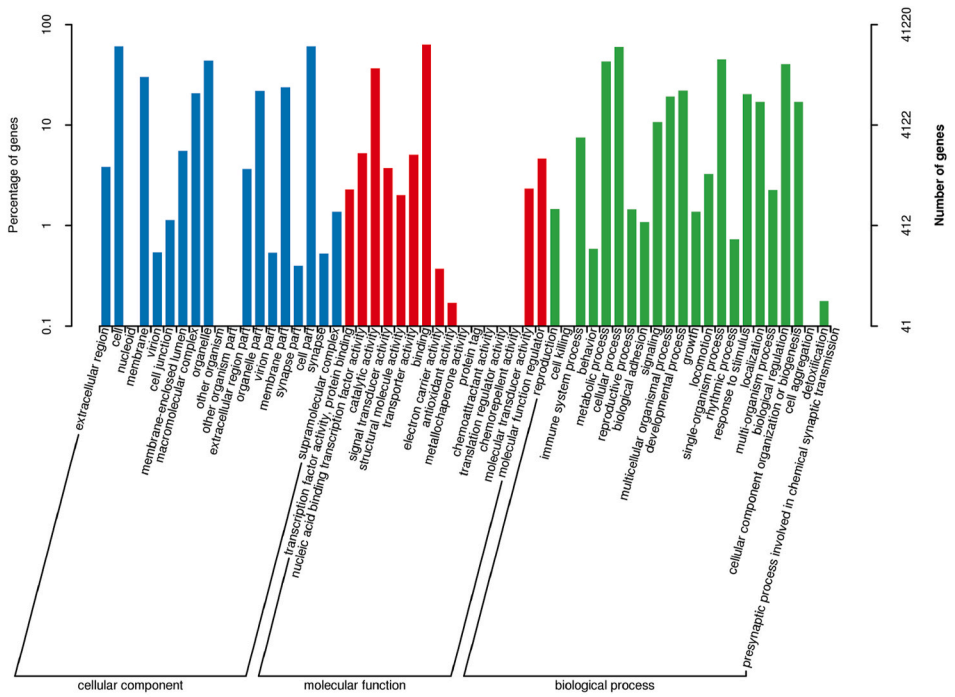

A

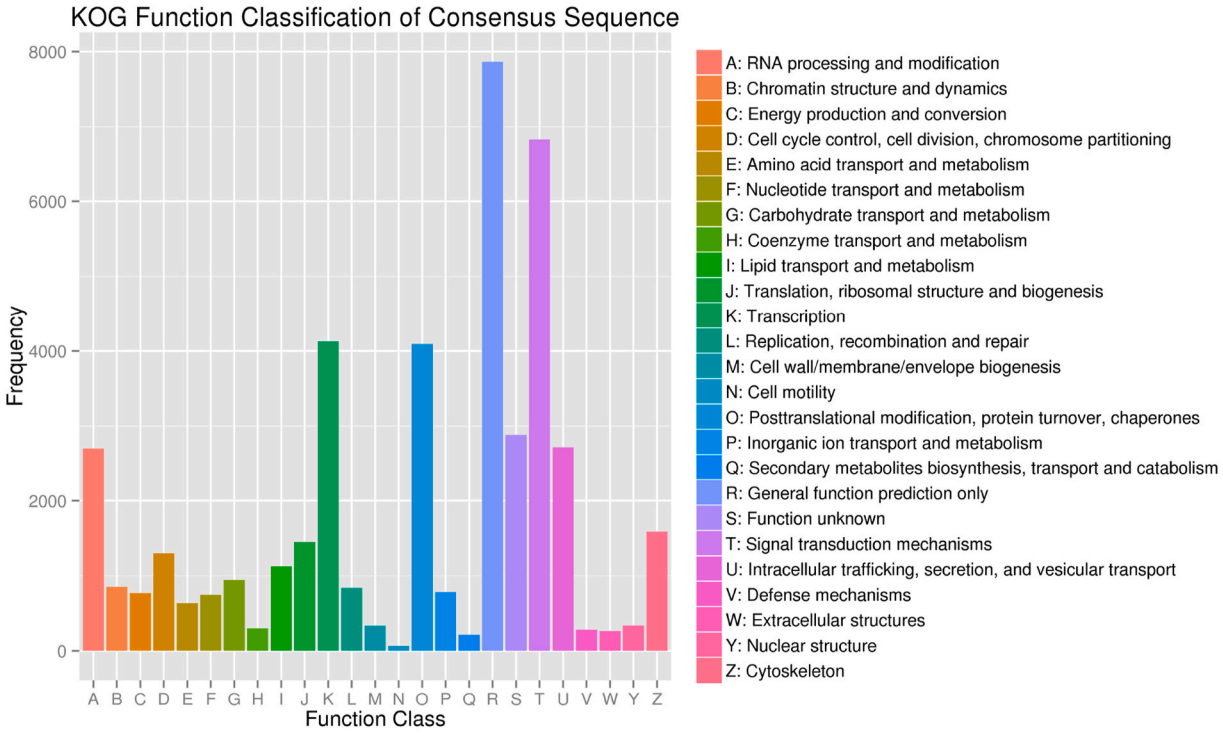

B

Fig. 2. GO annotation (A) and KOG functional annotation (B) of novel isoforms in 3 N full-length transcriptome. All GO annotations were classified into categories according to "cellular components", "biological processes" and "molecular functions". The abscissa shows gene functions and the ordinate is the number of transcripts with GO functions. In KOG annotations, the abscissa shows function class and the ordinate is the number of matched genes.

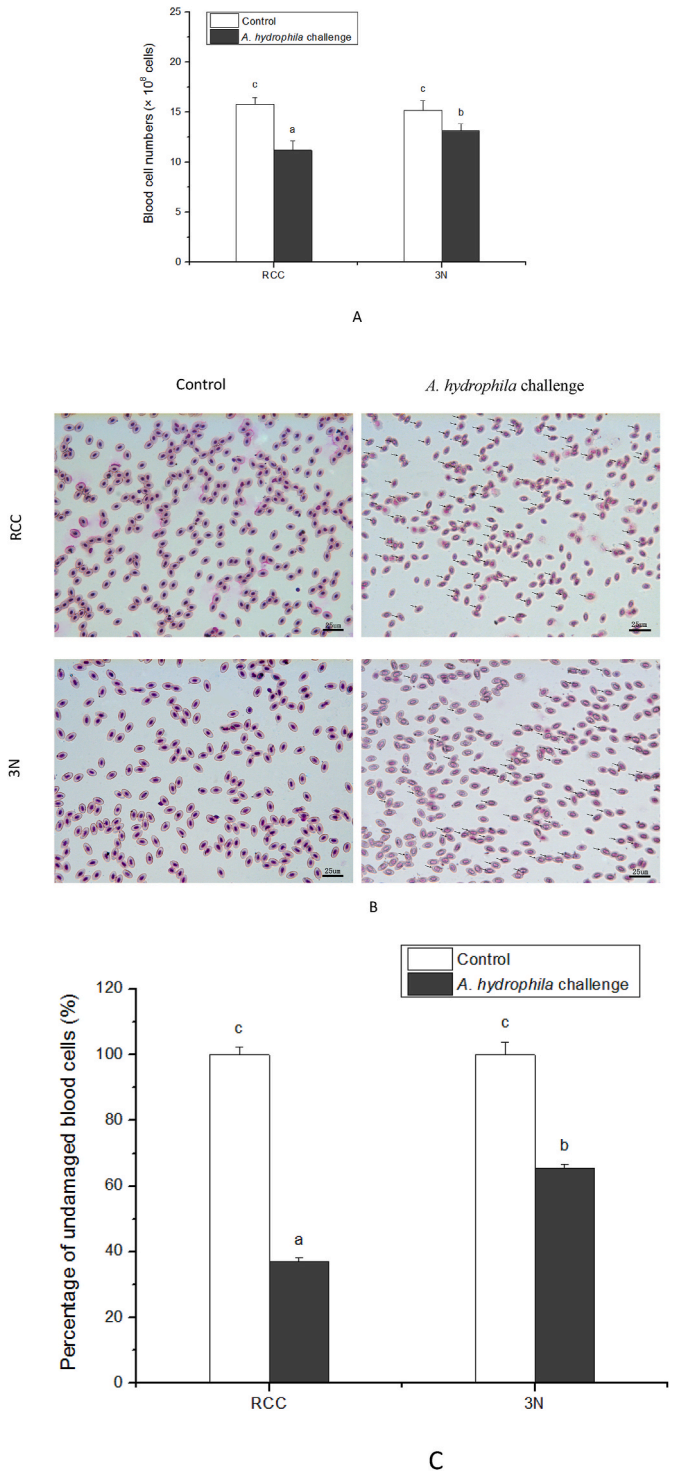

Fig. 3. Comparative analysis of blood parameters in RCC and 3 N following *A. hydrophila* challenge. (A) Blood cell count. A drop of diluted blood samples from each group was placed on the hemocytometer and counted by using a light microscope. (B–C) Blood cell morphology. Blood samples were stained with Giemsa staining kit. Following rinsing with deionized water, cover glasses were observed using a light microscope. The damaged blood cells were indicated by black arrows. The percentage of undamaged cells were calculated. The calculated data (mean ± SD) with different letters were significantly different ($P < 0.05$).

challenge, while it increased sharply in head kidney. In contrast, T-AOC levels increased dramatically in liver, head kidney, trunk kidney and spleen of 3 N following *A. hydrophila* challenge. In Fig. 4G, a dramatic increase of MDA amount was observed in liver, head kidney, trunk kidney and spleen of RCC and 3 N following *A. hydrophila* challenge.

3.4. Immune characterization of PBMCs after LPS stimulation

To detect the effect of LPS stimulation on isolated PBMCs of different ploidy cyprinid fish, CCK-8 assays were performed. As shown in Supplementary Fig. 3A, cell viability of PBMCs isolated from RCC began to decrease at 12 h following 1000 ng/ml of LPS stimulation, and then gradually decreased to 86.7% at 48 h. In contrast, cell viability of PBMCs isolated from 3 N decreased significantly to 88.9% at 48 h following 1000 ng/ml of LPS stimulation. In Fig. 5A-B, LPS stimulation could induce ROS production in PBMCs of RCC and 3 N, while cells pretreated with NAC could relieve LPS-induced ROS production. In Supplementary Fig. 3B-D, 1000 ng/ml of LPS stimulation could significantly alter $NADP^+$ and NADPH content in PBMCs isolated from RCC, while ratio of NADPH/$NADP^+$ peaked at 12 h. In Supplementary Fig. 3E-G, PBMCs of 3 N exhibited a sharp alternation of $NADP^+$ and NADPH content following 1000 ng/ml of LPS stimulation, while ratio of NADPH/$NADP^+$ peaked at 6 h, followed by a gradual decrease from 12 h to 48 h. In Supplementary Fig. 3H and a sharp increase of total SOD activity was observed at 12 h in PBMCs of RCC following LPS stimulation, followed by a gradual decrease from 12 h to 48 h. In contrast, PBMCs of 3 N exhibited a sharp decrease of total SOD activity after LPS stimulation from 6 h to 24 h, followed by a significant increase at 48 h (Supplementary Fig. 3I). In Supplementary Fig. 3J-K, MDA amount peaked at 6 h and 24 h in PBMCs of RCC and 3 N following LPS stimulation, respectively.

3.5. Clustering and function annotation of DEGs in different ploidy cyprinid fish

In order to explore the underlying molecular differences of different ploidy cyprinid fish following *A. hydrophila* infection, RNA-seq transcriptome was performed. RNA sequencing obtained approximately average 6.67 GB and 6.14 GB of data from RCC and 3 N with Q30 values higher than 97.2% and 98.53%, respectively. Based on PCA analysis, clear separations of control samples and *A. hydrophila* challenge samples were observed in RCCah vs RCCctl and 3Nah vs RCCctl (Supplementary Figs. 4A–B). As shown in Supplementary Fig. 4C-F, a total of 4507 and 1939 DEGs were identified in RCCah vs RCCctl and 3Nah vs 3Nctl, respectively. As shown in Supplementary Fig. 4G-H, 113 of the 2657 up-regulated DEGs in RCCah vs RCCctl were also among the gene differentially expressed in 3Nah vs 3Nctl, while 40 of 1850 down-regulated DEGs in RCCah vs RCCctl were also among the gene differentially expressed in 3Nah vs 3Nctl.

In Supplementary Fig. 5A-B, DEGs in RCCah vs RCCctl and 3Nah vs 3Nctl were annotated by GO. In biological process, the predominant portion of transcripts represented “regulation of transcription, DNA-templated” (311) in RCCah vs RCCctl, while “biological process” (137) were the most abundant sub-category in 3Nah vs 3Nctl. Within cellular component, the sub-category of “membrane” (1105 and 471) was the major portions of transcripts in RCCah vs RCCctl and 3Nah vs 3Nctl, respectively. In molecular function, the most abundant sub-category was “metal ion binding” (567 and 306) in RCCah vs RCCctl and 3Nah vs 3Nctl, respectively. The heatmap represented the clustering of RCCah vs RCCctl and 3Nah vs 3Nctl was shown in Fig. 6A. Nine GO terms were higher in RCCah vs RCCctl with the highest percentage of GO terms “lysozyme activity”. In contrast, seven GO terms were higher in 3Nah vs 3Nctl with the highest percentage of GO terms “regulation of response to DNA damage stimuli”.

To compare and investigate the mechanism linking *A. hydrophila*-induced DEGs of different ploidy cyprinid fish and their specific

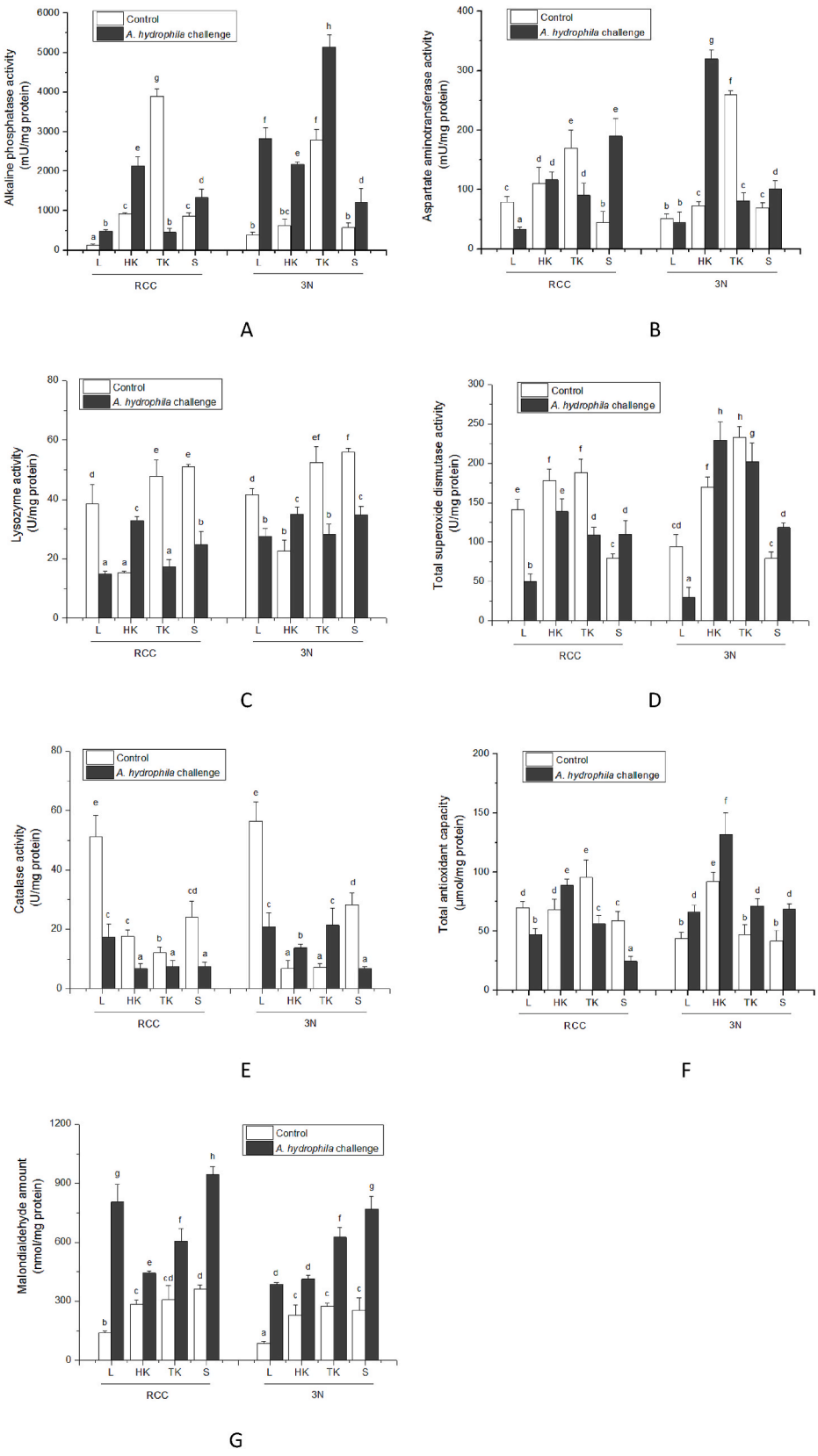

Fig. 4. Determination of enzymatic activity in liver, head kidney, trunk kidney and spleen of RCC and 3 N following *A. hydrophila* challenge. According to protocols of commercial kits, ALP (A), AST (B), LZM (C), total SOD (D), CAT (E), T-AOC (F) and MDA (G) were measured by using a microplate reader. The calculated data (mean ± SD) with different letters were significantly different ($P < 0.05$).

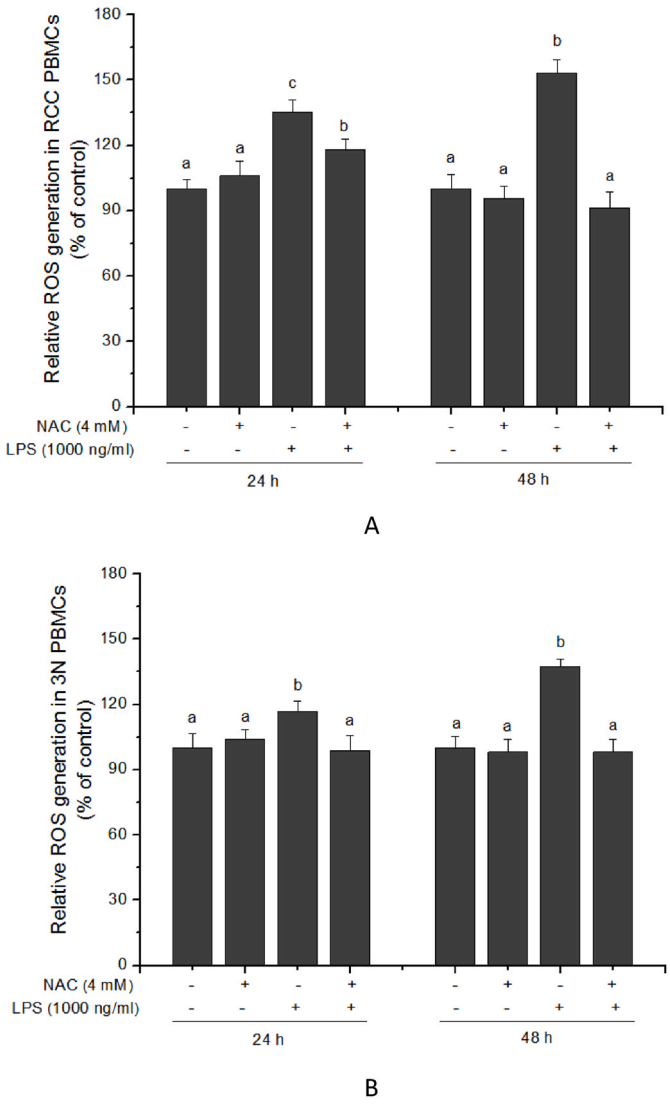

Fig. 5. Comparative analysis of ROS generation in isolated PBMCs from RCC (A) and 3 N (B) following LPS stimulation. Intracellular ROS content was stained with DCFH-DA probe. Isolated PBMCs were pretreated with 4 mM NAC for 30 min and incubated with 1000 ng/ml of LPS for 24 h and 48 h. The calculated data (mean ± SD) with different letters were significantly different ($P < 0.05$).

pathways, the obtained DEGs were used for pathway enrichment by KEGG analysis. In Supplementary Fig. 5C-D, DEGs in RCCah vs RCCctl and 3Nah vs 3Nctl belonged to six main classes, including "Cellular processes", "Environmental information processing", "Genetic information processing", "Human diseases", "Metabolism" and "Organismal systems". The most assigned subclass was "Cellular processes" in RCCah vs RCCctl, whereas the predominant assigned category was "Organismal systems". In addition, "NOD-like receptor (NLR) pathway" was significantly enriched with the most enriched DEGs in RCCah vs RCCctl and 3Nah vs 3Nctl (Fig. 6B and C). As shown in Supplementary Fig. 5E-F, the union of the top 50 enriched pathways of different ploidy cyprinid fish included 13 pathways. RCCah vs RCCctl and 3Nah vs 3Nctl exhibited the distinct enrichment patterns. To investigate the difference between *A. hydrophila* group and control group in different ploidy cyprinid fish in more detail, the up-regulated and down-regulated DEGs were mapped to KEGG pathways, respectively. As shown in Supplementary Fig. 5G, "NOD-like receptor pathway" and "Endocytosis" enriched the most numbers of up-regulated DEGs in RCCah vs RCCctl, while down-regulated DEGs were significantly enriched in "RNA transport",

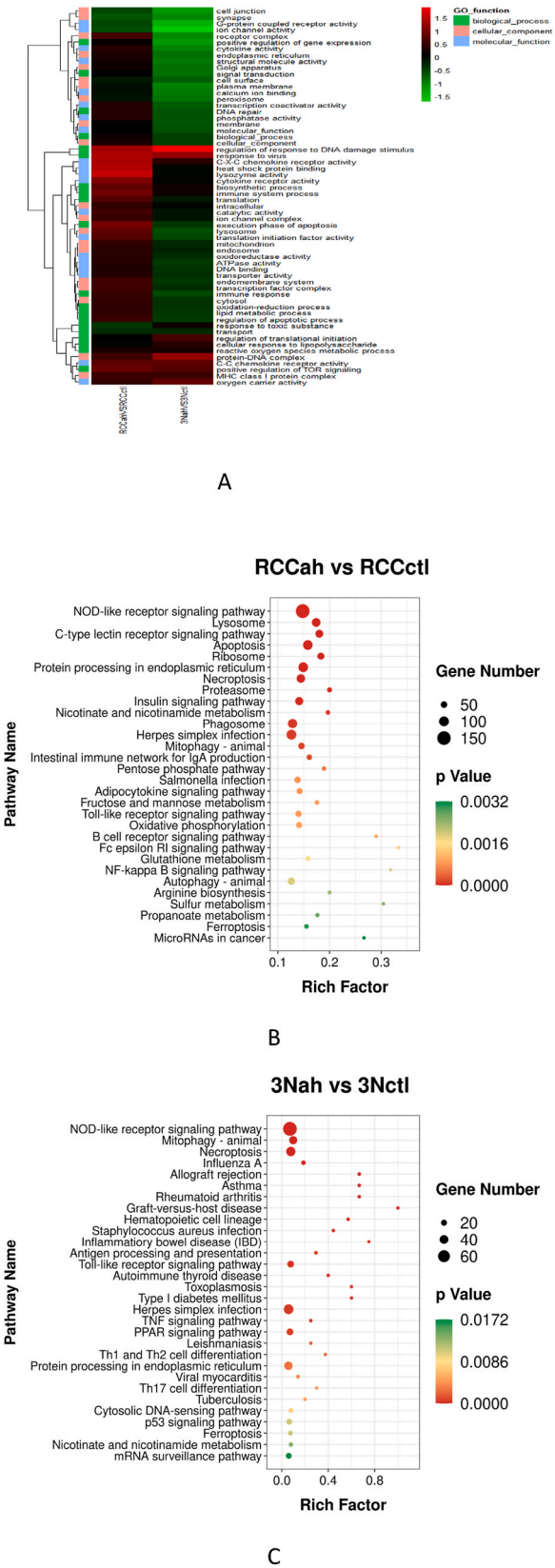

Fig. 6. GO annotation and KEGG pathway enrichment analysis. (A) HCA-heatmap showing percentage of GO terms was calculated by using $\log_{10}$ values. (B–C) Top 30 enriched KEGG pathways of DEGs in RCCah vs RCCctl and 3Nah vs 3Nctl.

"intestinal immune network for IgA production" and "Ribosome" (Supplementary Fig. 5H). In Supplementary Fig. 5I, KEGG terms of "Protein processing in endoplasmic reticulum", "RNA transport", "Autophagy" and "Spliceosome" enriched the most numbers of up-regulated DEGs in 3Nah vs 3Nctl, while down-regulated DEGs were significantly enriched in "Phagosome", "Tight junction", "Necroptosis", "Mitophagy", "Oxidative phosphorylation" and "Ribosome" (Supplementary Fig. 5J).

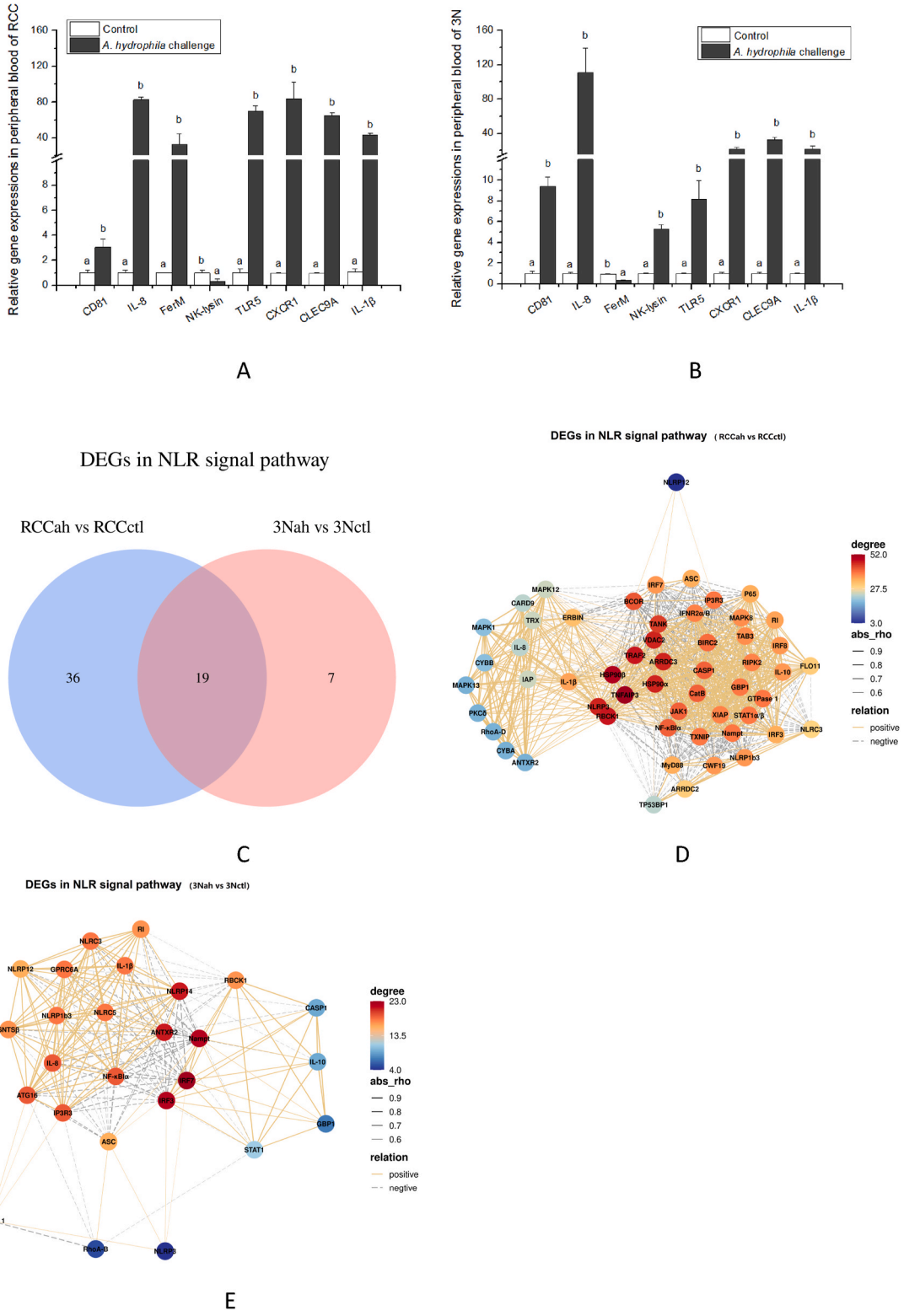

Fig. 7. qRT-PCR validation and co-expression network of DEGs. (A–B) Relative transcriptional level of selected 8 DEGs in peripheral blood of RCC and 3 N. The calculated data (mean ± SD) with different letters were significantly different ($P < 0.05$). (C) Venn diagram of DEGs in NLR signals of RCCah vs RCCctl and 3Nah vs 3Nctl. (D–E) Co-expression network of DEGs in NLR signals of RCCah vs RCCctl and 3Nah vs 3Nctl.

3.6. Gene co-expression networks of DEGs in different ploidy cyprinid fish

Furthermore, the differential expression profiles and co-expression networks of fifty-three core sets of genes involved in apoptosis, immunity, inflammation and cellular signals in RCCah vs RCCctl and 3Nah vs 3Nctl were shown in Supplementary Figs. 6A–C. Among them, eight DEGs were randomly selected for qRT-PCR assay. The results showed that eight genes exhibited different levels of expression in RCC and 3 N by comparing with their respective control (Fig. 7A and B). IL-8, CXCR1, TLR5, CLEC9A and IL-1β showed a higher expressions in RCC following *A. hydrophila* challenge, while down-regulation of NK-lysin expression was detected. In contrast, IL-8 exhibited the highest expression in 3 N following *A. hydrophila* challenge, followed by CLEC9A, IL-1β, CXCR1 and CD81, while decreased level of FerM was observed. In addition, the above immune-related genes were also detected in liver, head kidney, trunk kidney and spleen of RCC and 3 N. As shown in Supplementary Fig. 7A-H, the detected genes exhibited a tissue-specific expressions, while the up-regulated expressions of IL-1β, IL-8 and CLEC9A were observed in liver, head kidney, trunk kidney and spleen of RCC and 3 N following *A. hydrophila* challenge, suggesting that *A. hydrophila* challenge induced inflammatory response in a variety of immune-related tissues via a distinct regulatory manner.

3.7. Distinct immune activation of NLR signals in different ploidy cyprinid fish

In Fig. 7C, nineteen of fifty-five DEGs in NLR signals of RCCah vs RCCctl were also among the gene differentially expressed in 3Nah vs 3Nctl. The relative contents of DEGs in NLR signals of RCCah vs RCCctl and 3Nah vs 3Nctl were shown in Supplementary Figs. 8A–B. Forty-three genes were up-regulated in RCCah vs RCCctl, while twelve genes were down-regulated. In contrast, fifteen genes were up-regulated in 3Nah vs 3Nctl, while eleven genes were down-regulated. As shown in Fig. 7D-E, DEGs in NLR signals may exhibit a differentially co-expressed manner in RCCah vs RCCctl and 3Nah vs 3Nctl. In Supplementary Fig. 8C, above DEGs of NLR signals in RCCah vs RCCctl were predominantly enriched in caspase-1-dependent IL-1β secretion, IFN signals by activation of Janus kinase/signal transducer and activator of transcription (JAK/STAT) as well as activation of IL-1β and IL-8 through nuclear factor-κB (NF-κB) and mitogen activated protein kinase (MAPK) signals. In contrast, above DEGs of NLR signals in 3Nah vs 3Nctl were predominantly enriched in caspase-1-dependent IL-1β secretion and autophagy related protein 16 like protein 1 (ATG16L1)-mediated autophagy (Supplementary Fig. 8D). These results suggested that different ploidy cyprinid fish receiving *A. hydrophila* may elicit a distinct regulation of cellular response and signal transduction.

4. Discussion

A. hydrophila, a gram negative bacteria, is the major cause of outbreak in hemorrhagic septicemia in freshwater aquaculture. Aerolysin is one of significant virulent factors secreted by *A. hydrophila*, which can exert a direct binding activity to specific glycophosphatidylinositol (GPI)-anchored proteins on the surface of fish erythrocytes [25]. This interaction may facilitate the pore forming in cell membranes and cause a significant damage to fish erythrocytes, resulting in deep wound infection and internal organ lesion [26]. In this study, *A. hydrophila* challenge could dramatically decrease blood cell numbers and trigger a significant damage to blood cells of RCC and 3 N, while blood cell numbers and percentage of undamaged cells were consistently higher in 3 N following *A. hydrophila* challenge by comparing with those of RCC. These results implied that erythrocytes of 3 N elicited a higher resistance against *A. hydrophila*-induced cell damage in comparison with those of RCC.

In general, lymphoid organs, immune cells, humoral factors and cytokines are the key components that can confer protection against foreign organisms or substances, including bacteria, viruses, parasites and toxins, which may render fish higher sensitive to stressors [27]. Kidney and spleen are the predominant lymphoid tissues, participating in lymphocytes- and macrophages-mediated immune response [28], while liver can promote the synthesis and secretion of acute phase proteins that can alleviate the dispersal of infectious agents, mitigate tissue damage as well as eliminate invading pathogens [29]. However, acute bacterial infection can impair host immune defense, reduce phagocytic ability and dysregulate cellular signals, resulting in the delayed bacterial clearance [30]. LZM is involved in bacteriolytic process, phagocytic activity as well as activation of complement cascades [31]. ALP is a macrophage lysosomal marker enzyme that can lessen the toxicological effect of LPS and prevent inflammation [32]. AST can act as an important enzymatic marker of tissue damage in freshwater fish upon *in vitro* stimulation [33]. CD81 can modulate the adhesion, morphology, activation, proliferation of B and T cells [34]. CLEC9A is a C-type lectin-like receptor that can function as an activation receptor of immune cells and induce proinflammatory cytokine production [35]. IL-1β confers protection against gram-negative bacterial infection via inflammasome signals [36], while IL-8 can promote bacterial killing by neutrophils through CXCR1 [37]. FerM can participate in iron homeostasis, confer protection against oxidant-induced DNA damage and regulate the immune defense against microbial infection [38]. NK-lysin is an anti-microbial peptide of natural killer (NK) cells and cytotoxic T lymphocytes (CTLs), playing an important role in immune defense against pathogenic infection [39]. In this study, differential profiles of ALP, AST and LZM activities and immune-related genes were detected after acute *A. hydrophila* infection, but immune-related enzyme activities in 3 N were consistently higher than those of RCC, implying that 3 N receiving *A. hydrophila* challenge exhibited a stronger antibacterial activity by comparing with that of RCC.

A. hydrophila infection can increase oxidative stress in fish. The excessive accumulation of ROS level may exhibit an adverse effect on the organisms, leading to antioxidant imbalance and lipid peroxidation [40]. In general, antioxidant enzymes and compounds can directly mitigate cytokine-mediated toxicity [41], whereas severe oxidative stress can suppress antioxidant defense in fish [42]. In this study, 3 N receiving *A. hydrophila* infection showed a higher activities of T-AOC level, total SOD and CAT along with a lower MDA amount by comparing with those of RCC. In additional, bacterial LPS is a heat-stable endotoxin of gram-negative bacteria, which can directly induce inflammatory response by up-regulation of cytokines expressions in mammals [43]. Our previous studies have demonstrated that LPS stimulation could promote ROS generation, induce inflammatory signals and mediate mitochondrial apoptosis in cultured fish cells [44]. In this study, LPS stimulation could reduce cell viability, alter ratio of $NADPH/NADP^+$ and enhance MDA content in PBMCs isolated from RCC and 3 N, while LPS-induced ROS generation was consistently lower in PBMCs isolated 3 N by comparing with those of RCC. Taken together, these results suggested that 3 N undergoing inflammatory response may show the higher antioxidant capacity by comparing with that of RCC.

Vertebrate blood is involved in the central role in synchronize endocrine system to immune regulation, in which various forms of immune cells can participate in immune signals by directly generating hormones and cytokines under the control of central nervous system [45]. In general, fish blood parameters such as blood cell count, plasma glucose level, free hemoglobin, cortisol and antioxidant enzymatic activity can serve as potential biomarkers of environmental stressors and chemical toxins [46]. Additionally, exposure to stressors may also cause innate immune response in fish via various signal pathways, which may enable fish to cope with stress-evoked adverse effects [47]. However, the comparative mechanisms linking *A. hydrophila* infection to innate immune regulation in different ploidy cyprinid fish are still unclear.

In order to comprehensively understand the antibacterial response and innate immune mechanism of different ploidy cyprinid fish, we employed RNA-seq technology to investigate the transcriptome of RCC

and 3 N following *A. hydrophila* infection. In this study, NLR signals may appeared to play predominant roles in RCC and 3 N after *A. hydrophila* challenge. In general, recognition of invading bacteria may predominantly rely on the sensing of pathogen associated molecular patterns (PAMPs) by host pattern recognition receptors (PRRs), including TLRs, NLRs and RIG-I-like receptors (RLRs), then stimulating antimicrobial effector responses via the induction of proinflammatory cytokines [48]. As a clusters of immune sensors, NLR proteins can form inflammasomes and then mediate caspase-1-dependent IL-1β secretion, playing a critical role in bacteria-induce inflammatory response [49]. Moreover, NLR signal can also modulate NF-κB and MAPK signals, regulate the transcription of major histocompatibility complex (MHC) as well as activate autophagy-dependent antibacterial pathway by recruitment of ATG16L1 [50]. In this study, *A. hydrophila* challenge may promote caspase-1-dependent IL-1β secretion, enhance IFN signals by activation of JAK/STAT as well as activate the transcription of IL-1β and IL-8 through NF-κB and MAPK signals in RCC. In contrast, promotion of caspase-1-dependent IL-1β secretion and activation of ATG16L1-mediated antibacterial autophagy via NLR signals were observed in 3 N following *A. hydrophila* infection, suggesting that 3 N may exhibit the more specific antibacterial potentials to cope with *A. hydrophila* infection by comparing with that of RCC.

In summary, we compared blood cell count, blood cell morphology, enzymatic activity, gene expression profiles, co-expression network and signal transduction of different ploidy cyprinid fish. Our findings revealed that blood cells of 3 N showed a high resistance against *A. hydrophila*-induced cell damage by comparing with those of RCC. Acute *A. hydrophila* infection could alter non-specific immunity and antioxidant status along with elevated level of inflammatory modulators and MDA content in different ploidy cyprinid fish. In addition, we identified the distinct co-expression network and signal regulation of NLR proteins in RCC and 3 N after *A. hydrophila* challenge. Thus, the information presented in this study could provide a novel insight into differences in signal regulation of different ploidy cyprinid fish to cope with bacterial infection.

Declaration of competing interest

The authors declare that they have no conflict of interest.

Acknowledgements

This research was supported by the National Natural Science Foundation of China, China (grant no. 31902363), Hunan Provincial Natural Science Foundation of China, China (grant no.2021JJ40340) and the Doctoral Publishing Fund of Hunan Normal University, China (grant nos. 0531120-3680).

Appendix A. Supplementary data

Supplementary data to this article can be found online at https://doi.org/10.1016/j.fsi.2021.12.024.

References

[1] T. Benfey, Producing sterile and single-sex populations of fish for aquaculture, New Technol. Aquacult.: Improv. Prod. Effic. Qual. Environ. Manag. (2009) 143–164.
[2] G.M. Weber, M.A. Hostuttler, B.M. Cleveland, T.D. Leeds, Growth performance comparison of intercross-triploid, induced triploid, and diploid rainbow trout, Aquaculture 433 (2014) 85–93.
[3] A. Salmon, M.L. Ainouche, J.F. Wendel, Genetic and epigenetic consequences of recent hybridization and polyploidy in Spartina (Poaceae), Mol. Ecol. 14 (2005) 1163–1175.
[4] R.L. Rogers, T. Bedford, D.L. Hartl, Formation and longevity of chimeric and duplicate genes in Drosophila melanogaster, Genetics 181 (2009) 313–322.
[5] S. Liu, J. Luo, J. Chai, L. Ren, Y. Zhou, F. Huang, et al., Genomic incompatibilities in the diploid and tetraploid offspring of the goldfish× common carp cross, Proc. Natl. Acad. Sci. Unit. States Am. 113 (2016) 1327–1332.
[6] A. Šimková, L. Vojtek, K. Halačka, P. Hyršl, L. Vetešník, The effect of hybridization on fish physiology, immunity and blood biochemistry: a case study in hybridizing Cyprinus carpio and Carassius gibelio (Cyprinidae), Aquaculture 435 (2015) 381–389.
[7] Z. Li, Z.W. Wang, Y. Wang, J.F. Gui, Crucian Carp and Gibel Carp Culture. *Aquaculture In China: Success Stories and Modern Trends*, 2018, pp. 149–157.
[8] S. Liu, Y. Liu, G. Zhou, X. Zhang, C. Luo, H. Feng, et al., The formation of tetraploid stocks of red crucian carp× common carp hybrids as an effect of interspecific hybridization, Aquaculture 192 (2001) 171–186.
[9] D. Liu, S. Liu, C. You, L. Chen, Z. Liu, L. Liu, et al., Identification and expression analysis of genes involved in early ovary development in diploid gynogenetic hybrids of red crucian carp× common carp, Mar. Biotechnol. 12 (2010) 186–194.
[10] S. Chen, J. Wang, S. Liu, Q. Qin, J. Xiao, W. Duan, et al., Biological characteristics of an improved triploid crucian carp, Sci. China C Life Sci. 52 (2009) 733–738.
[11] N. dos Santos, M. Silva, Ad Vale, Fish and apoptosis: studies in disease and pharmaceutical design, Curr. Pharmaceut. Des. 14 (2008) 170–183.
[12] C. Yang, L. Liu, J. Liu, Z. Ye, H. Wu, P. Feng, et al., Black carp IRF5 interacts with TBK1 to trigger cell death following viral infection, Dev. Comp. Immunol. 100 (2019) 103426.
[13] B. Magnadottir, Immunological control of fish diseases, Mar. Biotechnol. 12 (2010) 361–379.
[14] C. Secombes, T. Wang, S. Hong, S. Peddie, M. Crampe, K. Laing, et al., Cytokines and innate immunity of fish, Dev. Comp. Immunol. 25 (2001) 713–723.
[15] H. Daskalov, The importance of Aeromonas hydrophila in food safety, Food Control 17 (2006) 474–483.
[16] P. Bhowmik, P.K. Bag, T.K. Hajra, R. De, P. Sarkar, T. Ramamurthy, Pathogenic potential of Aeromonas hydrophila isolated from surface waters in Kolkata, India, J. Med. Microbiol. 58 (2009) 1549–1558.
[17] T.J. Bowden, Modulation of the immune system of fish by their environment, Fish Shellfish Immunol. 25 (2008) 373–383.
[18] D. Marcogliese, The impact of climate change on the parasites and infectious diseases of aquatic animals, Rev. Sci. Technol. 27 (2008) 467–484.
[19] B. Liu, L. Xu, X. Ge, J. Xie, P. Xu, Q. Zhou, et al., Effects of mannan oligosaccharide on the physiological responses, HSP70 gene expression and disease resistance of Allogynogenetic crucian carp (Carassius auratus gibelio) under Aeromonas hydrophila infection, Fish Shellfish Immunol. 34 (2013) 1395–1403.
[20] N.-X. Xiong, S.-W. Luo, L.-F. Fan, Z.-W. Mao, K.-K. Luo, S.-J. Liu, et al., Comparative analysis of erythrocyte hemolysis, plasma parameters and metabolic features in red crucian carp (Carassius auratus red var) and triploid hybrid fish following Aeromonas hydrophila challenge, Fish Shellfish Immunol. 118 (2021) 369–384.
[21] D. Kim, B. Langmead, S.L. Salzberg, HISAT: a fast spliced aligner with low memory requirements, Nat. Methods 12 (2015) 357–360.
[22] G. Dotta, J.I.A. de Andrade, E.L.T. Gonçalves, A. Brum, J.J. Mattos, M. Maraschin, et al., Leukocyte phagocytosis and lysozyme activity in Nile tilapia fed supplemented diet with natural extracts of propolis and Aloe barbadensis, Fish Shellfish Immunol. 39 (2014) 280–284.
[23] R. Lulijwa, A.C. Alfaro, F. Merien, J. Meyer, T. Young, Advances in salmonid fish immunology: a review of methods and techniques for lymphoid tissue and peripheral blood leucocyte isolation and application, Fish Shellfish Immunol. 95 (2019) 44–80.
[24] A. Sadeghi, A.R. Bastin, H. Ghahremani, A.H. Doustimotlagh, The effects of rosmarinic acid on oxidative stress parameters and inflammatory cytokines in lipopolysaccharide-induced peripheral blood mononuclear cells, Mol. Biol. Rep. 47 (2020) 3557–3566.
[25] V. Singh, P. Somvanshi, G. Rathore, D. Kapoor, B. Mishra, Gene cloning, expression, and characterization of recombinant aerolysin from Aeromonas hydrophila, Appl. Biochem. Biotechnol. 160 (2010) 1985–1991.
[26] A.N. El Deen, M. Dorgham-Sohad, H. Hassan-Azza, A. Hakim, Studies on Aeromonas hydrophila in cultured Oreochromis niloticus at Kafr El Sheikh Governorate, Egypt with reference to histopathological alterations in some vital organs, World J. Fish Mar. Sci. 6 (2014) 233–240.
[27] B. Magnadóttir, Innate immunity of fish (overview), Fish Shellfish Immunol. 20 (2006) 137–151.
[28] C.M. Press, Ø. Evensen, The morphology of the immune system in teleost fishes, Fish Shellfish Immunol. 9 (1999) 309–318.
[29] C.J. Bayne, L. Gerwick, The acute phase response and innate immunity of fish, Dev. Comp. Immunol. 25 (2001) 725–743.
[30] Y.-C. Su, F. Jalalvand, J. Thegerström, K. Riesbeck, The interplay between immune response and bacterial infection in COPD: focus upon non-typeable haemophilus influenzae, Front. Immunol. 9 (2018) 2530.
[31] S. Saurabh, P. Sahoo, Lysozyme: an important defence molecule of fish innate immune system, Aquacult. Res. 39 (2008) 223–239.
[32] J.M. Bates, J. Akerlund, E. Mittge, K. Guillemin, Intestinal alkaline phosphatase detoxifies lipopolysaccharide and prevents inflammation in zebrafish in response to the gut microbiota, Cell Host Microbe 2 (2007) 371–382.
[33] K.A. Al-Ghanim, Effect of cypermethrin toxicity on enzyme activities in the freshwater fish Cyprinus carpio, Afr. J. Biotechnol. 13 (2014).
[34] S. Levy, S.C. Todd, H.T. Maecker, CD81 (TAPA-1): a molecule involved in signal transduction and cell adhesion in the immune system, Annu. Rev. Immunol. 16 (1998) 89–109.
[35] C. Huysamen, J.A. Willment, K.M. Dennehy, G.D. Brown, CLEC9A is a novel activation C-type lectin-like receptor expressed on BDCA3+ dendritic cells and a subset of monocytes, J. Biol. Chem. 283 (2008) 16693–16701.
[36] L. Franchi, N. Kamada, Y. Nakamura, A. Burberry, P. Kuffa, S. Suzuki, et al., NLRC4-driven production of IL-1β discriminates between pathogenic and

commensal bacteria and promotes host intestinal defense, Nat. Immunol. 13 (2012) 449–456.
[37] D. Hartl, P. Latzin, P. Hordijk, V. Marcos, C. Rudolph, M. Woischnik, et al., Cleavage of CXCR1 on neutrophils disables bacterial killing in cystic fibrosis lung disease, Nat. Med. 13 (2007) 1423–1430.
[38] D.A.S. Elvitigala, H. Premachandra, I. Whang, M.-J. Oh, S.-J. Jung, C.-J. Park, et al., A teleostean counterpart of ferritin M subunit from rock bream (Oplegnathus fasciatus): an active constituent in iron chelation and DNA protection against oxidative damage, with a modulated expression upon pathogen stress, Fish Shellfish Immunol. 35 (2013) 1455–1465.
[39] S.-W. Luo, N.-X. Xiong, Z.-Y. Luo, L.-F. Fan, K.-K. Luo, Z.-W. Mao, et al., A novel NK-lysin in hybrid crucian carp can exhibit cytotoxic activity in fish cells and confer protection against Aeromonas hydrophila infection in comparison with Carassius cuvieri and Carassius auratus red var, Fish Shellfish Immunol. 116 (2021) 1–11.
[40] M.P. Lesser, Oxidative stress in marine environments: biochemistry and physiological ecology, Annu. Rev. Physiol. 68 (2006) 253–278.
[41] S. Lortz, M. Tiedge, T. Nachtwey, A.E. Karlsen, J. Nerup, S. Lenzen, Protection of insulin-producing RINm5F cells against cytokine-mediated toxicity through overexpression of antioxidant enzymes, Diabetes 49 (2000) 1123–1130.
[42] N.-X. Xiong, S.-W. Luo, Z.-W. Mao, L.-F. Fan, K.-K. Luo, S. Wang, et al., Ferritin H can counteract inflammatory response in hybrid fish and its parental species after Aeromonas hydrophila infection, Comp. Biochem. Physiol. C Toxicol. Pharmacol. (2021) 109174.
[43] R.-B. Yang, M.R. Mark, A. Gray, A. Huang, M.H. Xie, M. Zhang, et al., Toll-like receptor-2 mediates lipopolysaccharide-induced cellular signalling, Nature 395 (1998) 284–288.
[44] S.-W. Luo, N.-X. Xiong, Z.-Y. Luo, K.-K. Luo, S.-J. Liu, C. Wu, et al., Effect of Lipopolysaccharide (LPS) stimulation on apoptotic process and oxidative stress in fibroblast cell of hybrid crucian carp compared with those of Carassius cuvieri and Carassius auratus red var, Comp. Biochem. Physiol. C Toxicol. Pharmacol. 248 (2021) 109085.
[45] G. Csaba, The immuno-endocrine system: hormones, receptors and endocrine function of immune cells. The packed-transport theory, Adv. Neuroimmune Biol. 1 (2011) 71–85.
[46] H. Roche, G. Bogé, Fish blood parameters as a potential tool for identification of stress caused by environmental factors and chemical intoxication, Mar. Environ. Res. 41 (1996) 27–43.
[47] J.B. Jørgensen, The innate immune response in fish, Fish Vacc. 1 (2014) 84–102.
[48] S. Kumar, H. Ingle, D.V.R. Prasad, H. Kumar, Recognition of bacterial infection by innate immune sensors, Crit. Rev. Microbiol. 39 (2013) 229–246.
[49] P.J. Sansonetti, A. Phalipon, J. Arondel, K. Thirumalai, S. Banerjee, S. Akira, et al., Caspase-1 activation of IL-1β and IL-18 are essential for Shigella flexneri–induced inflammation, Immunity 12 (2000) 581–590.
[50] T.A. Kufer, P.J. Sansonetti, NLR functions beyond pathogen recognition, Nat. Immunol. 12 (2011) 121–128.